

XXI INT. CONF. ON LOW TEMPERATURE PHYSICS IN PRAGUE, 8-14 AUGUST 1996

Unconventional Pairing in Heavy Fermion Metals *J. A. Sauls^a and D. Rainer^b^a Department of Physics & Astronomy, Northwestern University, Evanston, IL 60208, USA.^b Physikalisches Institut, Universität Bayreuth, D-95440 Bayreuth, Germany.

The Fermi-liquid theory of superconductivity is applicable to a broad range of systems that are candidates for unconventional pairing, *e.g.* heavy fermion, organic and cuprate superconductors. Ginzburg-Landau theory provides a link between the thermodynamic properties of these superconductors and Fermi-liquid theory. The multiple superconducting phases of UPt_3 illustrate the role that is played by the Ginzburg-Landau theory in interpreting these novel superconductors. Fundamental differences between unconventional and conventional anisotropic superconductors are illustrated by the unique effects that impurities have on the low-temperature transport properties of unconventional superconductors. For special classes of unconventional superconductors the low-temperature transport coefficients are *universal*, i.e. independent of the impurity concentration and scattering phase shift. The existence of a universal limit depends on the symmetry of the order parameter and is achieved at low temperatures $k_B T \ll \gamma \ll \Delta_0$, where γ is the bandwidth of the impurity induced Andreev bound states. In the case of UPt_3 thermal conductivity measurements favor an E_{1g} or E_{2u} ground state. Measurements at ultra-low temperatures should distinguish different pairing states.

1. Introduction

Theoretical investigation of *unconventional* pairing began with the publication by Anderson and Morel [1], “Generalized Bardeen-Cooper-Schrieffer States and the Proposed Low-Temperature Phase of ^3He ”. They studied the physical consequences of BCS pairing with non-zero angular momentum, including superfluid phases with spontaneously broken time-reversal symmetry. When superfluidity was discovered [2] in ^3He it was immediately clear that this was not a conventional s-wave BCS superfluid because there was more than one superfluid phase. Further evidence for unconventional pairing came from many experimental results and shortly after their discovery the three superfluid phases of ^3He were undisputedly identified as p-wave spin-triplet superfluids.

The search for *unconventional superconductivity*, the metallic analog of superfluidity in ^3He , was given a boost by the discoveries of superconductivity in the class of heavy-fermion metals [3], particularly in the U-based compounds of UBe_{13} , UPt_3 , URu_2Si_2 , UNi_2Al_3 , and UPd_2Al_3 . Unusual temperature dependences of the heat capacity, penetration depth, and sound absorption led to conjectures that these materials were unconventional superconductors [4]. Much more experimental information is now avail-

able, and there is consensus that some heavy-fermion superconductors (if not all of them) show unconventional pairing. Interest in unconventional superconductivity expanded further with reports of several experiments on cuprate superconductors that supported earlier predictions [5] of “d-wave pairing”.

A rigorous classification of superconductors by the angular momentum of the Cooper pairs (i.e. s-wave, p-wave, d-wave pairing, etc.) is not appropriate in crystalline materials because angular momentum is not a good quantum number. However, the terms “d-wave pairing”, etc. are often used interchangeably with “unconventional pairing” for states in which the pairing amplitude spontaneously breaks one or more symmetries of the crystalline phase, i.e. $\mathcal{R} * \Delta(\mathcal{R} * \mathbf{p}_f) \neq \Delta(\mathbf{p}_f)$, where $\mathcal{R} \in \mathcal{G} = \mathcal{G}_{spin} \times \mathcal{G}_{space} \times \mathcal{T} \times \mathcal{U}_{gauge}$ represents an operation of the full symmetry group \mathcal{G} other than a pure gauge transformation, and

$$\Delta_{\alpha\beta}(\mathbf{p}_f) \sim \langle a_{\mathbf{p}_f\alpha} a_{-\mathbf{p}_f\beta} \rangle, \quad (1)$$

* We thank the Max Planck Gesellschaft and the Alexander von Humboldt Stiftung for support. JAS also acknowledges partial support from the NSF through the Science and Technology Center for Superconductivity (DMR 91-20000).

is the equal-time pair amplitude, or order parameter, that describes BCS-type superconductors. Note that \mathbf{p}_f is the momentum of a quasiparticle on the Fermi surface and α, β are the spin labels of the paired quasiparticles. Fermion statistics requires that the pair amplitude obey the anti-symmetry condition, $\Delta_{\alpha\beta}(\mathbf{p}_f) = -\Delta_{\beta\alpha}(-\mathbf{p}_f)$.

Essentially all of the candidates for unconventional superconductivity, including the heavy-fermion and cuprate superconductors, have inversion symmetry. This has an important consequence; the pairing interaction that drives the superconducting transition decomposes into even- and odd-parity sectors [6, 7]. Thus, $\Delta_{\alpha\beta}(\mathbf{p}_f)$ necessarily has even or odd parity unless there is a second superconducting instability into a state with different parity.

The d-wave model for the cuprates

Superconductivity in the high T_c cuprates is generally believed to result from pairing correlations within the CuO planes. Knight shift measurements below T_c indicate that the pairs form spin singlets [8], and therefore even-parity orbital states. Unlike the superfluid phases of ^3He the cuprates exhibit a single superconducting phase. The absence of multiple superconducting phases in the cuprates suggests that the orbital pairing state belongs to one of the four one-dimensional representations illustrated in Fig. 1, for tetragonal crystal symmetry.

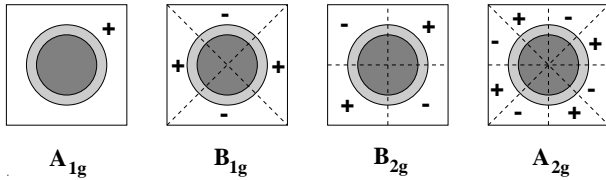


Fig. 1. Graphical representation the 1-dimensional basis functions for even-parity tetragonal superconductors. The broken reflection planes and the signs of the pairing state are indicated.

The popular $d_{x^2-y^2}$ model for the cuprate superconductors [9] belongs to the B_{1g} representation. This state breaks the reflection symmetries for the (110) planes. As a result the order parameter changes sign in momentum space as indicated in Fig. 1, and the excitation gap $|\Delta(\mathbf{p}_f)|$ has nodes in the (110) direction on the Fermi surface. Both features lead to novel transport properties in the superconducting state at very low temperatures [10, 11].

Multi-component Models of UPt₃

Considerable evidence in support of an unconventional pairing state in the heavy-fermion ma-

terials has accumulated from specific heat, upper critical field and various transport measurements, all of which show anomalous properties compared to those of conventional superconductors (see Refs. ([4, 12]) for original references). However, some of the strongest evidence for unconventional superconductivity comes from the multiple superconducting phases of UPt₃ [13, 14], which are a strong indication of a multi-component pairing amplitude that necessarily breaks one or more symmetries of the normal state.

There are several important features of the H-T phase diagram. (i) There are two zero-field superconducting phases with a difference in transition temperatures of $\Delta T_c/T_c \simeq 0.1$. (ii) A change in slope of the upper critical field (a ‘kink’ in H_{c2}^\perp) is observed for $\mathbf{H} \perp \hat{\mathbf{c}}$. (iii) There are three flux phases, and the phase transition lines separating the flux phases appear to meet at a tetracritical point for all orientations of \mathbf{H} relative to $\hat{\mathbf{c}}$. Three basic models that have been proposed to explain the phases of UPt₃.

1. *Multi-component Order Parameter coupled to a Symmetry-Breaking Field (SBF)*. These are models based on a primary order parameter belonging to a higher dimensional representation of the symmetry group of the normal state. For UPt₃, which has hexagonal (D_{6h}) symmetry, there are four 2D representations, $E_{1g(u)}$ and $E_{2g(u)}$, with basis functions that transform like, $\mathcal{Y}_{E_{1\pm}} \sim p_z(p_x \pm ip_y)$ for the even-parity E_{1g} representation, and $\mathcal{Y}_{E_{2\pm}} \sim p_z(p_x \pm ip_y)^2$ for the odd-parity E_{2u} states. The order parameter is then a complex two-component vector $\vec{\eta} = (\eta_1, \eta_2)$ that transforms according to the relevant 2D representation, and is related to the pairing amplitude by

$$\Delta(\mathbf{p}_f) = \eta_+ \mathcal{Y}_{E_{1,2+}} + \eta_- \mathcal{Y}_{E_{1,2-}}, \quad (2)$$

with $\eta_{\pm} = \eta_1 \pm i\eta_2$. Multiple superconducting phases correspond to different stationary solutions of the free energy functional for $\vec{\eta}$.

The small splitting of the double transition in UPt₃ ($\Delta T_c/T_c \simeq 0.1$) suggests the presence of a small symmetry breaking energy scale and an associated lifting of a degeneracy of the possible superconducting states belonging to the 2D representation [15, 16, 17]. The second zero-field transition just below T_c in UPt₃, as well as the anomalies observed in the upper and lower critical fields, have been explained in terms of a weak symmetry breaking field (SBF) that lowers the crystal symmetry from hexagonal to orthorhombic, and consequently reduces the 2D E_2 (or E_1) representation to two 1D representations with slightly different transition temperatures.

The key point is that right at T_c all states belonging to the 2D representation are degenerate, thus any SBF that couples to $\vec{\eta}$ in second-order, and prefers a particular state, will dominate very near T_c . At lower temperatures the SBF energy scale, ΔT_c , is a small perturbation compared to the fourth-order terms in the fully developed superconducting state and one recovers the results of the GL theory for the 2D representation with small perturbations to the order parameter.

The phase diagram determined by ultrasound velocity measurements indicates that the phase boundary lines meet at a tetracritical point for both $\mathbf{H} \parallel \hat{c}$ and $\mathbf{H} \perp \hat{c}$. This has been argued to contradict the GL theory based on a 2D order parameter [18, 19, 20]. The difficulty arises from gradient terms of the form, $[(D_x \eta_1)(D_y \eta_2)^* + (D_x \eta_2)(D_y \eta_1)^* + c.c.]$, that couple the two components of the order parameter. These terms lead to ‘level repulsion’ effects in the linearized GL differential equations which prevent the crossing of two $H_{c2}(T)$ curves, corresponding to different superconducting phases. This feature of the 2D model has spawned alternative models, designed specifically to eliminate the ‘level repulsion’ effect [19, 20], and to a more specific version of the 2D model coupled to a SBF based on the E_{2u} representation [21].

2. Accidental degeneracy of two order parameters. These models are based on *two* primary order parameters that are unrelated by symmetry, i.e. belong to different irreducible representations of the symmetry group, and are accidentally nearly degenerate. The model of two 1D representations, A_2 and B_1 (“AB model”) is a specific example [20]. The motivation behind this model is that by choosing the two representations appropriately one can guarantee that the ‘level repulsion’ terms in the Ginzburg-Landau equations for H_{c2} are absent by symmetry [18, 20]. What is required is that the two order parameters corresponding to the two irreducible representations, have different signatures under reflection, or parity. In this case the second-order gradient coupling between the two order parameters vanishes, and the apparent tetracritical point is present for all field orientations. The drawback is that the accidental degeneracy models provide no explanation for the near degeneracy of T_c , the observed correlation between ΔT_c and the AFM order parameter, or the pressure-temperature phase diagram.

3. Enlarged Symmetry Group Models. These are *hybrid* models that assume an accidental degeneracy in the form of a larger symmetry group for the nor-

mal phase than one expects based on the atomic and electronic structure of the crystal. A SBF is then invoked to lift the degeneracy of a higher dimensional representation for the larger symmetry group. By assuming a larger group than D_{6h} one can again eliminate the ‘level repulsion’ terms exactly in the GL limit by judicious choice of the primary representation. Two different versions of the enlarged symmetry group model have been proposed; one based on an enlarged orbital symmetry group and the other based on the assumption of *no* spin-orbit coupling. The orbital model starts from the full rotation group, $\mathcal{G}_{space} = SO(3)$ and produces multiple phases by crystal field splitting of the pairing states [22]. This is a flexible model, but there is no strong evidence to support treating UPt₃ as an isotropic material, even approximately; and there is no explanation for the correlation between the AFM order and the multiple superconducting phases.

The spin-channel version of this model [19] assumes a symmetry group composed of independent orbital and spin rotations with $\mathcal{G}_{spin} = SU(2)$. The multi-component order parameter in this model corresponds to the three spin-triplet amplitudes defined in terms of a 3D complex \vec{d} vector. The ‘level repulsion’ terms are absent for a 1D orbital representation. Coupling of the AFM order parameter to the \vec{d} vector is proposed to split the transitions for the different triplet sub-states. This model requires weak spin-orbit coupling, which is at odds with theoretical estimates for the spin-orbit coupling energy [12]. Furthermore, weak spin-orbit coupling is in contradiction with the observation of anisotropic Pauli limiting [23]; a spin-triplet order parameter with weak spin-orbit coupling would not exhibit Pauli limiting for any field orientation (see also Ref.[21]).

More on the SBF model for UPt₃

In the absence of accidental near degeneracy, a SBF is essential for lifting the degeneracy of the pairing states near T_c and producing multiple superconducting phases [16, 17, 24]. A natural candidate for a SBF in UPt₃ is the AFM order in the basal plane [25]. In this case the GL functional includes a coupling of the AFM order parameter to the superconducting order parameter; $\mathcal{F}_{SBF}[\vec{\eta}] = \varepsilon M_s^2 \int d^3x (|\eta_1|^2 - |\eta_2|^2)$, where M_s is the AFM order parameter and the coupling parameter εM_s^2 determines the magnitude of the splitting of the superconducting transition. The analysis of this GL theory, including the SBF, is given in Ref. ([16]); some of the main results summarized below.

A double transition is predicted with a splitting of T_c proportional to $\Delta T_c \propto M_s^2$. Support for the SBF model of the double transition comes from pressure studies of the superconducting and AFM phase transitions. Heat capacity measurements by Trappmann, *et al.* [26] show that both zero-field transitions are suppressed under hydrostatic pressure, and that the double transition disappears at $p_* \simeq 4 \text{ kbar}$. Neutron scattering experiments reported by Hayden, *et al.* [27] show that AFM order disappears on the same pressure scale, at $p_c \simeq 3.2 \text{ kbar}$.

The low temperature phase ($T < T_{c*}$) is predicted to have broken \mathcal{T} symmetry. This phase is doubly degenerate: $\vec{\eta}_{\pm} \sim (a(T), \pm i b(T))$, reflecting the two orientations of the internal orbital momentum of the ground state.

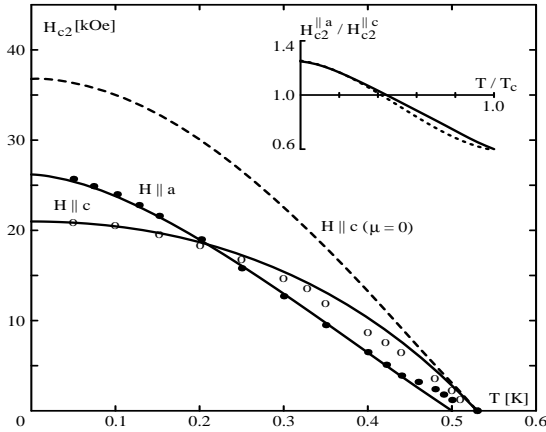


Fig. 2. Calculations of H_{c2}^{\perp} and H_{c2}^{\parallel} vs. T for an odd-parity, triplet pairing state with the \vec{d} vector locked to the \hat{c} direction [28]. The inset shows the ratio $H_{c2}^{\parallel}/H_{c2}^{\perp}$ vs. T/T_c . Note that H_{c2}^{\parallel} is suppressed by paramagnetism ($\mu \approx \mu_B$) at low temperatures, while H_{c2}^{\perp} is independent of the paramagnetic coupling. The data of Shivaram, *et al.* [23] are shown as the open and closed circles.

Another key feature of the UPt_3 phase diagram is the unusual anisotropy of H_{c2} shown in Fig. 2. The low-temperature anisotropy is explained in terms of anisotropic Pauli limiting of an odd-parity, spin-triplet state with the \vec{d} -vector parallel to the \hat{c} direction [28]. This restricts one to the E_{2u} or E_{1u} symmetry classes among the four possible 2D representations.

The SBF is essential for producing an apparent tetracritical point, and at a semi-quantitative level, can account for the magnitudes of the slopes near the tetracritical point [21, 29]. However, there are open

questions regarding both the nature of the AFM order and its coupling to superconductivity [30]. As this model for UPt_3 illustrates, GL theory provides a central link between experiments, in this case the phase diagram, and the more microscopic Fermi-liquid theory which we discuss below.

2. Fermi-Liquid Theory of Heavy Fermion Superconductivity

Conduction electrons in metals interact strongly with each other and with the lattice. These interactions lead to correlations among the electrons, and we have to view conduction electrons, in general, as a system of correlated fermions. A particularly important system of strongly correlated electrons are the conduction electrons of heavy fermion metals. There is strong evidence that these heavy electrons form a Landau Fermi liquid at low temperatures, and that their superconducting states are well described by the Fermi liquid theory of superconductivity. In the following we give a brief introduction to this theory, then discuss recent applications to transport in heavy fermion superconductors with unconventional pairing.

Landau showed that an ensemble of strongly interacting fermions may be described by a distribution function for quasiparticle excitations, and that this distribution function obeys a classical transport equation, the Boltzmann-Landau transport equation. It took more than 10 years after Landau's theory of normal Fermi liquids, and the breakthrough in the theory of superconductivity by BCS, to establish a complete Fermi-liquid theory of superconductivity. Earlier general theories of superconductivity lacked the quasiclassical aspects of Landau's Fermi-liquid theory. The first complete quasiclassical (QC) theory of superconductivity was formulated in a series of publications by Eilenberger [31], Larkin and Ovchinnikov [32] and Eliashberg [33]. It is presented and discussed in several review articles [34, 35, 36]. The quasiclassical theory allows one to calculate all superconducting phenomena of interest, including transition temperatures, excitation spectra, Josephson effects, vortex structures, the electromagnetic response, etc. In this theory the dynamical degrees of freedom of electronic quasiparticles are described partly by classical mechanics, and partly by quantum statistics. The classical degrees of freedom are the motion in \mathbf{p} - \mathbf{R} phase space; i.e. quasiparticles move along classical trajectories. Quantum degrees of freedom are the spin of a quasiparticle and the particle-hole degree of freedom, which form

a four-dimensional Hilbert space of “internal degrees of freedom”.

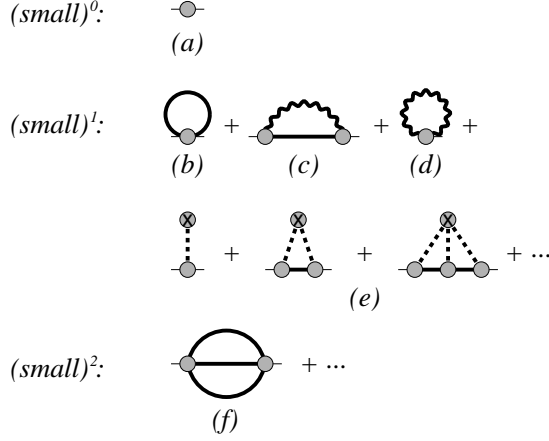


Fig. 3. Leading order self-energy diagrams of Fermi-liquid theory. The vertices (shaded circles) represent the sum of all high-energy processes and give rise to interactions between the quasiparticles (smooth propagator lines), phonons (wiggly propagator lines) and impurities (dashed lines). The order in the parameter ‘small’ $\sim \epsilon/E_f$ is indicated for each diagram.

Derivations of the Boltzmann-Landau transport equation from first principles [37, 38] use many-body Green’s function techniques, and lead to explicit expressions for the various terms of the transport equation in terms of self-energies. The self-energies describe the effects of electron-electron, electron-phonon and electron-impurity scattering. The complete set of diagrams for the leading order self-energies are shown in Fig. 3; the filled circles are vertices representing the effective lattice potential, which determines the quasiparticle Fermi surface and Fermi velocities, as well as quasiparticle-quasiparticle, quasiparticle-phonon, and quasiparticle-impurity interactions. We follow Landau and consider these vertices as phenomenological parameters of the Fermi-liquid model, but in principle they can be obtained from the full many-body theory. The selection of leading order self-energies holds for the normal and the superconducting states. The vertices are not affected in leading order by the superconducting transition; superconductivity affects only the electron propagators. The special achievement of Eilenberger, Larkin, Ovchinnikov, and Eliashberg was to convert Dyson’s equations for the electron propagators into transport equations for quasiclassical propagators. The resulting equations define the quasiclassical theory of superconductivity.

The central equation of the quasiclassical theory is the transport equation for the quasiclassical Keldysh propagator, \hat{g}^K ,

$$(\epsilon\hat{\tau}_3 - \hat{v} - \hat{\sigma}^R) \otimes \hat{g}^K - \hat{g}^K \otimes (\epsilon\hat{\tau}_3 - \hat{v} - \hat{\sigma}^A) - \hat{\sigma}^K \otimes \hat{g}^A + \hat{g}^R \otimes \hat{\sigma}^K + i\hbar\mathbf{v}_f \cdot \nabla \hat{g}^K = 0. \quad (3)$$

The retarded, advanced, and Keldysh propagators, $\hat{g}^{R,A,K}(\mathbf{p}_f, \mathbf{R}; \epsilon, t)$, as well as the self-energies, $\hat{\sigma}^{R,A,K}(\mathbf{p}_f, \mathbf{R}; \epsilon, t)$, and the external potentials, $\hat{v}(\mathbf{p}_f, \mathbf{R}, t)$, are 4×4 Nambu matrices, acting on the 4D Hilbert space of internal degrees of freedom. The \otimes -product stands for the usual 4×4 -matrix product and a product in the energy-time variables. Details of this compact notation are explained in the reviews of the quasiclassical theory [34, 35, 36]. The determination of \hat{g}^K from the transport equation requires knowledge of the external potentials, the advanced, retarded and Keldysh self-energies, and the advanced and retarded quasiclassical propagators. These propagators are auxiliary quantities which in general have no direct physical interpretation, except in the adiabatic limit [34] where they determine the local quasiparticle density of states. The retarded and advanced propagators are solutions of

$$[\epsilon\hat{\tau}_3 - \hat{v} - \hat{\sigma}^{R,A}, \hat{g}^{R,A}]_{\otimes} + i\hbar\mathbf{v}_f \cdot \nabla \hat{g}^{R,A} = 0. \quad (4)$$

The physically relevant set of solutions of Eqs. (3) and (4) must satisfy the normalization conditions,

$$\hat{g}^{R,A} \otimes \hat{g}^{R,A} = -\pi^2 \hat{1}, \quad \hat{g}^R \otimes \hat{g}^K + \hat{g}^K \otimes \hat{g}^A = 0. \quad (5)$$

Measurable quantities such as the charge current density, $\mathbf{j}(\mathbf{R}, t)$, can be calculated from the diagonal components of the quasiclassical propagator, \hat{g}^K . For example, the charge current density is given by

$$\mathbf{j}(\mathbf{R}, t) = \int \frac{2 d^2 \mathbf{p}_f}{(2\pi)^3 |\mathbf{v}_f|} \int \frac{d\epsilon}{4\pi i} e\mathbf{v}_f g^K(\mathbf{p}_f, \mathbf{R}; \epsilon, t). \quad (6)$$

The quasiclassical equations (3)-(5) are supplemented by self-consistency equations for the quasiclassical self-energies. These equations are shown in diagrammatic notation in Fig. 3. They include, for example, the “gap equation”, which is the self-consistency equation for the off-diagonal self-energy. Explicit forms of the quasiclassical self-energies can be found in Refs. [34, 35, 36].

The quasiclassical theory is especially well suited for studying unconventional superconductors. Some of the results of the theory for conventional s-wave superconductors are simply generalized to unconventional superconductors. For example, the density

of states $N(\mathbf{p}_f; \epsilon)$ of a homogeneous spin-singlet superconductor in equilibrium has the standard BCS form, $N(\mathbf{p}_f; \epsilon) = N_f \Re[\epsilon / \sqrt{|\Delta|^2 - \epsilon^2}]$, but with the isotropic gap $|\Delta|$ replaced by an anisotropic gap, $|\Delta(\mathbf{p}_f)|$, for each point on the Fermi surface.

However, inhomogeneous and non-equilibrium situations exhibit more striking differences between conventional and unconventional superconductors that reflect both the broken symmetries of the order parameter and the coherence properties of the superconducting state.

Particle-Hole Coherence in QC Theory

Of special importance for understanding superconducting phenomena are the quantum-mechanical “internal degrees of freedom”, the *spin* and the *particle-hole* degrees of freedom of an electron. Quantum coherence between particle excitations and hole excitations is a key feature of the BCS theory of superconductivity and the origin of all non-classical effects in superconductors (e.g. supercurrents, coherence factors in transition amplitudes, Andreev reflection, etc.). Particle-hole coherence is incorporated into the quasiclassical theory by grouping particle excitations (occupied one-electron states above the Fermi energy) and hole excitations (empty one-electron states below the Fermi energy) into a doublet. For clean superconductors, and for long wavelength spatial variations, $\xi_0 = \hbar v_f / 2\pi T_c \gg \hbar / p_f$, we can make a quasiclassical envelope approximation for the Bogoliubov amplitudes; the resulting particle and hole amplitudes obey Andreev’s equation,[42]

$$(\epsilon \hat{\tau}_3 - \hat{\Delta}(\mathbf{p}_f, \mathbf{R})) \vec{\varphi}_{\mathbf{p}_f} + i\hbar \mathbf{v}_f \cdot \nabla \vec{\varphi}_{\mathbf{p}_f} = 0, \quad (7)$$

where $\vec{\varphi}_{\mathbf{p}_f} = (u_{\mathbf{p}_f}, v_{\mathbf{p}_f})$ are the quasiclassical particle (u) and hole (v) amplitudes. Andreev’s equation is a first-order differential equation for excitations propagating along straight-line trajectories determined by the Fermi velocity $\mathbf{v}_f(\mathbf{p}_f)$ at a point \mathbf{p}_f on the Fermi surface. In the superconducting state, the order parameter $\hat{\Delta}(\mathbf{p}_f, \mathbf{R})$ mixes the normal-state excitations coherently into two branches of particle-like ($\mathbf{p}_f \cdot \mathbf{v}_+ > 0$) and hole-like ($\mathbf{p}_f \cdot \mathbf{v}_- < 0$) excitations.

Coherence between particle and hole excitations leads to dramatic effects on the excitation spectrum of an unconventional superconductor in the vicinity of an impurity or a surface. Consider an excitation that is incident on a specular surface from the bulk region of a superconductor with broken reflection symmetry perpendicular to the plane of the

interface. When an excitation reflects off the surface elastically its momentum shifts to a new point on the Fermi surface, $\mathbf{p}_f \rightarrow \underline{\mathbf{p}}_f$. Thus, the incident and reflected wavepacket propagate through different order parameter fields, $\Delta(\mathbf{p}_f, \mathbf{R})$ vs. $\Delta(\underline{\mathbf{p}}_f, \mathbf{R})$. As a result, surface scattering generally leads to Andreev scattering, a process of “retro-reflection” in which a particle-like excitation undergoes branch conversion into a hole-like excitation with reversed group velocity. Bound states may occur at energies for which the phases of multiply-reflected particle- and hole-like excitations interfere constructively.

The effects of a surface on particle-hole coherence is most pronounced if the scattering induces a change in sign of the order parameter along the classical trajectory. This occurs for a $d_{x^2-y^2}$ superconductor with a (110) surface, an E_{1g} or E_{2u} order parameter and a surface normal to the $\hat{\mathbf{c}}$ axis. If a sign change of the order parameter occurs along the trajectory, then a zero-energy bound state forms at the surface with equal amplitudes for the particle and hole components [39]. These states are expected to give rise to zero-bias anomalies in the conductance for NIS tunnel junctions [40, 41, 43].

Impurity-induced Andreev bound states

The novel effects of impurities in unconventional superconductors, including pairbreaking, can be understood in similar terms. Fermion bound states are formed by impurity-induced Andreev scattering. Figure 4 illustrates the connection between potential scattering and the development of an Andreev bound state for s-wave impurities in the $d_{x^2-y^2}$ model; similar physical processes apply to unconventional models of the heavy fermion superconductors. Impurities give rise to elastic scattering of states near the Fermi surface, with transition matrix elements given by $u(\mathbf{p}_f, \mathbf{p}'_f)$. The scattering amplitude is determined by the t -matrix,

$$\hat{t}^{R,A}(\mathbf{p}_f, \mathbf{p}'_f, \mathbf{R}; \epsilon, t) = u(\mathbf{p}_f, \mathbf{p}'_f) + N_f \int d\mathbf{k}_f u(\mathbf{p}_f, \mathbf{k}_f) \hat{g}^{R,A}(\mathbf{k}_f, \mathbf{R}; \epsilon, t) \otimes \hat{t}^{R,A}(\mathbf{k}_f, \mathbf{p}'_f, \mathbf{R}; \epsilon, t) \quad (8)$$

The t -matrix sums two types of repeated scattering processes to all orders: (i) potential scattering processes with a change in momentum, but no change in the internal state, and (ii) Andreev scattering processes, i.e. branch conversion with no change in momentum, but reversal of the group velocity. The Andreev processes are *induced* by the sign changes of the order parameter that result from scattering around

the Fermi surface as shown in Fig. 4. Bound states also form from impurity-induced Andreev scattering, with an energy that depends on the scattering phase shift. Neglecting broadening effects from the continuum states above the gap, the bound state energy is given by $\epsilon_{\text{bound}} = \Delta_0 \cos \delta_0$. However, the continuum excitations are nearly gapless in the vicinity of the nodes of $\Delta(\mathbf{p}_f)$, so bound states at finite energy are broadened into resonances. For strong scattering the bound state occurs near zero energy and the resonance width is narrow; e.g. in the unitarity limit the impurity bound states appear at $\epsilon = 0$ and are sharp.

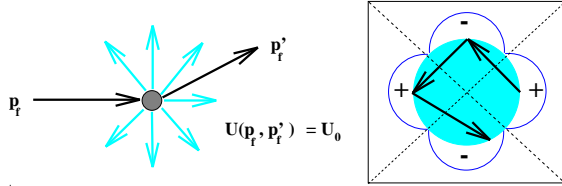


Fig. 4. Scattering of quasiparticles by an impurity induces Andreev scattering, and for unconventional pairing states the formation of Andreev bound states or resonances.

In a dilute alloy a finite density of impurities leads to a finite density of impurity states, an Andreev band [44]. The impurity bandwidth and density of states can be calculated from the self-consistent \hat{t} -matrix and the leading order impurity self-energy terms (diagrams 3e). The bandwidth is given by

$$\gamma = \Gamma_u \frac{\langle \gamma (|\Delta(\mathbf{p}_f)|^2 + \gamma^2)^{-1/2} \rangle}{\cot^2 \delta_0 + \langle \gamma (|\Delta(\mathbf{p}_f)|^2 + \gamma^2)^{-1/2} \rangle^2}, \quad (9)$$

where $\Gamma_u = n_{\text{imp}}/\pi N_f$ is the maximum impurity scattering rate in the normal state for a fixed concentration, n_{imp} , of impurities and $\langle \dots \rangle$ is an average over the Fermi surface. In the unitarity limit the impurity bandwidth is $\gamma \simeq \sqrt{\pi \Gamma_u / 2 \Delta_0} \sim \sqrt{n_{\text{imp}}}$.

For $\gamma < \epsilon \ll \Delta_0$ the low energy spectrum is dominated by continuum excitations in the vicinity of the nodal lines; for the E_{1g} and E_{2u} models of UPt_3 $N(\epsilon) \approx N_f(\epsilon/\Delta_0)$. Below $\epsilon \approx \gamma$ the impurity band dominates with $N(\epsilon) \simeq N(0) \approx N_f(\gamma/\Delta_0)$. These two contributions to the spectrum also give rise to different features in the transport properties of the heavy fermion superconductors [10, 45]. To calculate the transport coefficients in the superconducting state we need the Keldysh propagator for these branches of the excitation spectrum. Linear response functions for electrical and thermal transport in strong-coupling, dirty and unconventional superconductors are derived from the quasiclassical transport equations in Refs. [36, 10, 45].

3. Thermal Conductivity of UPt_3 - E_{2u} Model

The anisotropic thermal conductivity coefficients for the E_{2u} model are shown in Fig. 5 as a function of temperature, and compared with the data of Lussier, et al. [46] for $T \geq 0.1T_c$. The fits of the E_{2u} model to the low temperature region, $0.1 < T/T_c < 0.5$ are very good for both directions of heat flow. More detailed analysis shows that both the E_{2u} and E_{1g} pairing states give excellent fits to the thermal conductivity for $T > 0.1T_c$, and that ultra-low temperature (i.e. $T < \gamma$) heat transport measurements and impurity studies should distinguish these pairing states [11].

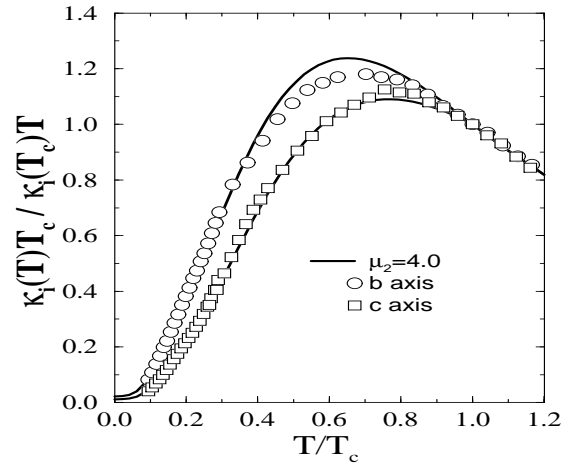


Fig. 5. The normalized thermal conductivity of the E_{2u} ground state [11] compared with the data of Ref. [46]. The impurity scattering rate is $\Gamma_0 = 0.01\pi T_{c0}$ and the phase shift is $\delta_0 = 90^\circ$. The slope and curvature parameters are $\mu_1 = 2.0$ and $\mu_2 = 4.0$.

Ultra-Low Temperature Heat Transport

Signatures the pairing symmetry arise from both the low-energy continuum states and the impurity-induced Andreev band. This novel metallic band deep in the superconducting state gives rise to *universal* transport coefficients for $k_B T \ll \gamma$ [10]. Whether or not a universal limit develops at low temperatures depends sensitively on the nodal structure of the excitation gap. Both the E_{1g} and E_{2u} models for the order parameter of UPt_3 lead to an excitation gap with a nodal line in the basal plane and point nodes along the $\pm \hat{c}$ directions [47]. The difference in the excitation spectrum for these two states is that the gap opens linearly for small angles away from the \hat{c} direction for the E_{1g} order parameter, but quadratically for E_{2u} order parameter; $|\Delta_{E_{1g}}(\vartheta)| \simeq \Delta_0 \mu_1 |\vartheta|$ and $|\Delta_{E_{2u}}(\vartheta)| \simeq \Delta_0 \mu_2 |\vartheta|^2$. This difference is reflected in $\lim_{T \rightarrow 0} \kappa_c/T$, which is universal for the E_{2u}

model, but non-universal for the E_{1g} model [11],

$$\kappa_c/T \simeq \frac{\pi^2}{3} N_f^2 v_f^2 \left(\frac{\gamma}{\mu_1^2 \Delta_0^2} \right) \left(1 + \frac{a_{E_{1g}}^2 T^2}{\gamma^2} \right) \quad (10)$$

$$\kappa_c/T \simeq \frac{\pi^2}{3} N_f^2 v_f^2 \left(\frac{1}{2\mu_2 \Delta_0} \right) \left(1 + \frac{a_{E_{2u}}^2 T^2}{\gamma^2} \right) \quad (11)$$

For heat flow in the basal plane the thermal conductivity is determined by the line node, and is universal for *both* E_{1g} and E_{2u} pairing states. The leading temperature corrections to κ/T are given by a Sommerfeld expansion for $T < \gamma < T_c$. The T^3 corrections are non-universal and in the unitarity limit, $\gamma^2 \propto n_{\text{imp}}$, so the coefficient of the T^3 term scales as $1/n_{\text{imp}}$ for the E_{2u} state and $1/\sqrt{n_{\text{imp}}}$ for the E_{1g} state. Observed universality for $T \ll \gamma$ and the scaling of the T^3 correction with n_{imp} would be strong tests of the symmetry of the order parameter.

We thank M. J. Graf, D. W. Hess, and S.-K. Yip for many contributions to the work reported here.

REFERENCES

- [1] P. W. Anderson and P. Morel, Phys. Rev. **123**, 1911 (1961).
- [2] D. D. Osheroff, R. C. Richardson, and D. M. Lee, Phys. Rev. Lett. **28**, 885 (1972).
- [3] F. Steglich *et al.*, Phys. Rev. Lett. **43**, 1892 (1979).
- [4] H. Ott *et al.*, Jpn. J. Appl. Phys. **S26**, 1882 (1987).
- [5] N. E. Bickers, D. J. Scalapino, and R. T. Scalettar, Int. Journ. Mod. Phys. **B1**, 687 (1987).
- [6] P. Anderson, Phys. Rev. **B30**, 4000 (1984).
- [7] G. Volovik and L. Gor'kov, Sov. Phys. JETP Lett. **39**, 674 (1984).
- [8] M. Takigawa, P. C. Hammel, R. H. Heffner, and Z. Fisk, Phys. Rev. **B39**, 7371 (1989).
- [9] D. Scalapino, Phys. Rep. **250**, 329 (1995).
- [10] M. J. Graf, M. Palumbo, D. Rainer, and J. A. Sauls, Phys. Rev. B **52**, 10588 (1995).
- [11] M. J. Graf, S.-K. Yip, and J. A. Sauls, J. Low Temp. Phys. - Rapid Comm. **102**, 367 (1996).
- [12] R. Heffner and M. Norman, Comm. Cond. Matt. Phys. **17**, 361 (1996).
- [13] G. Bruls *et al.*, Phys. Rev. Lett. **65**, 2294 (1990).
- [14] S. Adenwalla *et al.*, Phys. Rev. Lett. **65**, 2298 (1990).
- [15] R. Joynt, Sup. Sci. Tech. **1**, 210 (1988).
- [16] D. Hess, T. Tokuyasu, and J. A. Sauls, J. Phys. Cond. Matt. **1**, 8135 (1989).
- [17] K. Machida and M. Ozaki, J. Phys. Soc. Jpn **58**, 2244 (1989).
- [18] I. Luk'yanchuk, J. de Phys. **I1**, 1155 (1991).
- [19] K. Machida and M. Ozaki, Phys. Rev. Lett. **66**, 3293 (1991).
- [20] D. Chen and A. Garg, Phys. Rev. Lett. **70**, 1689 (1993).
- [21] J. Sauls, Adv. Phys. **43**, 113 (1994).
- [22] M. Zhitomirskii and I. Luk'yanchuk, Sov. Phys. JETP Lett. **58**, 131 (1993).
- [23] B. Shivaram, T. Rosenbaum, and D. Hinks, Phys. Rev. Lett. **57**, 1259 (1986).
- [24] R. Joynt, V. Mineev, G. Volovik, and Zhitomirskii, Phys. Rev. **B42**, 2014 (1990).
- [25] G. Aeppli *et al.*, Phys. Rev. Lett. **60**, 615 (1988).
- [26] T. Trappmann, H. v. Löhneysen, and L. Taillefer, Phys. Rev. **B43**, 13714 (1991).
- [27] S. Hayden, L. Taillefer, C. Vettier, and J. Flouquet, Phys. Rev. **B46**, 8675 (1992).
- [28] C. Choi and J. Sauls, Phys. Rev. Lett. **66**, 484 (1991).
- [29] K. Park and R. Joynt, Phys. Rev. B **53**, 12346 (1996).
- [30] B. Lussier. *et al.*, unpublished (1996).
- [31] G. Eilenberger, Z. Physik **214**, 195 (1968).
- [32] A. I. Larkin and Y. N. Ovchinnikov, Sov. Phys. JETP **28**, 1200 (1969).
- [33] G. M. Eliashberg, Sov. Phys. JETP **34**, 668 (1972).
- [34] J. W. Serene and D. Rainer, Phys. Rep. **101**, 221 (1983).

- [35] A. I. Larkin and Y. N. Ovchinnikov, in *Nonequilibrium Superconductivity*, edited by D. Langenberg and A. Larkin (Elsevier Science Publishers, Amsterdam, 1986), pp. 493-542.
- [36] D. Rainer and J. A. Sauls, in *Superconductivity: From Basic Physics to New Developments*, edited by P. N. Butcher and Y. Lu (World Scientific, Singapore, 1995), pp. 45-78.
- [37] L. D. Landau, Sov. Phys. JETP **5**, 70 (1959).
- [38] G. M. Eliashberg, Zh. Eksp. Teor. Fiz. **15**, 1151 (1962).
- [39] L. J. Buchholtz and G. Zwicknagl, Z. Phys. **B23**, 5788 (1981).
- [40] C. R. Hu, Phys. Rev. Lett. **72**, 1526 (1994).
- [41] Y. Tanaka and S. Kashiwaya, Phys. Rev. Lett. **74**, 3451 (1995).
- [42] A. Andreev, Sov. Phys. JETP **19**, 1228 (1964).
- [43] L. Buchholtz, M. Palumbo, D. Rainer, and J. A. Sauls, J. Low Temp. Phys. **101**, 1099 (1995).
- [44] C. Choi and P. Muzikar, Phys. Rev. **B36**, 54 (1987).
- [45] M. J. Graf, S.-K. Yip, J. A. Sauls, and D. Rainer, Phys. Rev. **B53**, 15147 (1996).
- [46] B. Lussier, B. Ellman, and L. Taillefer, Phys. Rev. B **53**, 5145 (1996).
- [47] M. Norman, Physica **C194**, 205 (1992).